Available online at www.sciencedirect.com
ScienceDirect
Journal of Organometallic Chemistry 692 (2007) 5245–5255
Journal of Organometallic Chemistry
www.elsevier.com/locate/jorganchem

Hydrosilylation, hydrocyanation, and hydroamination of ethene catalyzed by bis(hydrido-bridged)diplatinum complexes: Added insight and predictions from theory

Constantinos A. Tsipis *, Christos E. Kefalidis

Laboratory of Applied Quantum Chemistry, Department of Chemistry, Aristotle University of Thessaloniki, 541 24 Thessaloniki, Greece

Received 25 June 2007; received in revised form 7 August 2007; accepted 7 August 2007
Available online 14 August 2007

Abstract

Details on the reaction mechanism of the catalytic cycle of hydrosilylation, hydrocyanation and hydroamination of ethene catalyzed by bis(hydrido-bridged)diplatinum complexes were obtained with the aid of DFT by calculating the relevant intermediates and transition state structures. The catalytically "active" species identified are the 16e coordinatively unsaturated mononuclear $[Pt(X)(H)(PH_3)(\eta^2\text{-}C_2H_4)]$ ($X = SiH_3$, CN, NH_2) species formed upon addition of the ethene molecule on the monomeric $[Pt(X)(H)(PH_3)]$ precursors. All crucial reaction steps encapsulated in the entire catalyzed courses have been scrutinized. The following three steps are found to be critical for these catalytic reactions: (i) the migration of the hydride to the acceptor C atom of the coordinated ethene substrate, (ii) the reductive elimination of the final product and (iii) the oxidative addition process that regenerates the catalyst with activation barriers of 13.1, 16.5 and 13.3 kcal/mol for hydrosilylation, 7.1, 31.0 and 2.8 kcal/mol for hydrocyanation and 11.7, 39.7 and 39.0 kcal/mol for hydroamination reactions. In all cases the rate-determining step is that of the reductive elimination of the final product having always the highest activation barrier. The overall catalytic processes are exergonic with the calculated exergonicities being −13.5 (−8.0), −16.1 (−10.4) and −38.8 (−46.7) kcal/mol for the hydrosilylation, hydrocyanation and hydroamination of ethene, respectively, at the B3LYP (CCSD(T)) levels of theory. According to energetic span of the cycle called δE, which determines the frequency of the catalytic cycle, we found that the catalytic efficiency of the hydrido-bridged diplatinum complexes follows the trend: hydrocyanation ≈ hydrosilylation > hydroamination.

Keywords: Hydrosilylation; Hydroamination; Hydrocyanation; DFT calculations; Bis(hydrido-bridged)diplatinum(II) complexes; Mechanistic aspects

1. Introduction

The electrophilic activation of alkenes by transition-metal catalysts is a fundamental step in a variety of catalytic processes of potential industrial interest. The majority of catalytic reactions that involve the platinum mediated activation of alkenes lead to the net addition of an E–H bond (E = C, Si, N, or O) across a C=C bond [1]. The key step is the reaction of a metal–olefin complex with a nucleophile to give a β-substituted metal–alkyl species. This transformation can in principle proceed through an inner-sphere or an outer-sphere mechanism, with different implications for catalyst design. The generally preferred mechanism for Pt-catalyzed additions to alkenes (Scheme 1a) involves the coordination of a C=C bond to an electrophilic Pt center that activates the alkene toward outer-sphere attack by a protic nucleophile Nu–H. The newly formed Pt–C bond is then cleaved by protonolysis to regenerate the catalyst.

The alternate inner-sphere mechanism (Scheme 1b), involves coordination of the nucleophile (Nu) first to Pt through deprotonation of Nu–H and ligand exchange. The key step in the inner-sphere mechanism is the

* Corresponding author. Tel.: +030 2310 997851.
E-mail address: tsipis@chem.auth.gr (C.A. Tsipis).

0022-328X/$ - see front matter © 2007 Elsevier B.V. All rights reserved.
doi:10.1016/j.jorganchem.2007.08.007

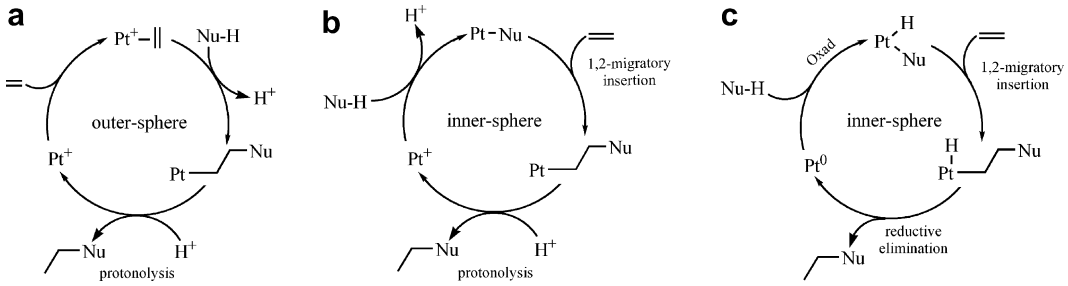

Scheme 1. (a) Catalytic addition of Nu–H to an alkene by outer-sphere nucleophilic attack and protonolysis of the Pt–C bond. (b) Catalytic addition of Nu–H to an alkene by metalation, insertion, and protonolysis. (c) Catalytic addition of Nu–H to an alkene by oxidative addition (Oxad), insertion, and reductive elimination.

1,2-migratory insertion of a bound olefin into the Pt–Nu bond. A variation on the inner-sphere mechanism, involving a Pt(II)/Pt(0) redox couple, is also possible as it is shown in Scheme 1c. Here, initial oxidative addition (Oxad) of NuH to Pt(0) is followed by olefin insertion into the Pt–Nu bond. The resulting Pt–C bond is cleaved by a C–H reductive elimination rather than by protonolysis. While this mechanism is generally preferred for more electron-rich metals such as rhodium and iridium, and is almost exclusively invoked for transition-metal-catalyzed olefin hydrogenation and hydrosilylation, several lines of evidence, suggest that platinum-catalyzed additions of protic C–H or N–H nucleophiles more likely proceed by the outer-sphere electrophilic activation mechanism [1] shown in Scheme 1.

Recently, we provided a comprehensive and consistent picture of the catalytic cycles of the hydrosilylation, hydrocyanation and hydroamination of ethyne catalyzed by bis(hydrido-bridged)diplatinum complexes using electronic structure calculation techniques at the DFT level of theory [2]. In the current paper, we focused on the mechanistic details of the hydrosilylation, hydrocyanation and hydroamination of ethene catalyzed by bis(hydrido-bridged)diplatinum complexes. Nonlocal, gradient-corrected DFT, in conjunction with effective core potentials and valence basis sets, was utilized to locate all of the stationary points in the catalytic cycle. Moreover, high level, ab initio CCSD(T) method was employed to compute the energies of all the stationary points, to refine the energetic profile of the potential energy hypersurface. In particular, the present study seeks to extend the understanding of the intricate structural and energetic details of the olefin hydrosilylation, hydrocyanation and hydroamination processes. To assess the efficiency of the catalytic cycles under turnover conditions, the recently suggested [3] energy span quantity, δE, (the energy difference between the summit and deepest species of the cycles) has been applied.

2. Computational methods

The entire gas-phase potential energy surfaces (PES) for the olefin hydrosilylation, hydrocyanation and hydroamination processes constituting the respective catalytic cycles were determined at the B3LYP and CCSD(T)//B3LYP levels of theory. To reduce the computational complexity of the calculations, a PH_3 model was used in lieu of PPh_3 and related phosphane ligands typically found in experimental systems. Although PMe_3 has been shown to be a better model for PPh_3 than PH_3 [4], it was felt that the additional degrees of freedom arising from the methyl groups would inhibit a thorough investigation of the different isomers and conformers of each species participating in the catalytic cycle. In addition, this approach has been tested in several previous theoretical studies and proven to provide correct relative trends in the reactivity of transition-metal phosphane complexes [5–7]. In all DFT calculations the B3LYP hybrid density functional that comprised of Becke's hybrid gradient-corrected exchange functional [8] and the gradient-corrected correlation functional of Lee, Yang, and Parr [9] was employed. This functional provides good descriptions of reaction profiles, including geometries, heats of reactions, and barrier heights [10–12]. The LANL2DZ basis set was used for the Pt atoms combined with the BS II basis set of Frenking et al. [13], that incorporates the Hay and Wadt [14] small-core relativistic effective core potential (ECP) with the optimized valence basis functions contracted to [441/2111/21] and the 6-31G(d,p) basis set for the rest of the non metal atoms. We will denote the computational approach used as B3LYP/LANL2DZ+BSII(Pt)∪6-31G**(L). In all computations no constrains were imposed on the geometry. The nature of the extrema (local minima or transition states) was checked by analytical frequency calculations. The computed electronic energies, the enthalpies of reactions, $\Delta_R H_{298}$ and the activation energies, $\Delta G^{\ddagger}_{298}$, were corrected to constant pressure and 298 K, for zero point energy (ZPE) differences and for the contributions of the translational, rotational and vibrational partition functions. Furthermore, because the B3LYP approach underestimates activation barriers [15], to obtain more reliable activation barriers single-point energy calculations were also performed on the B3LYP/LANL2DZ+BSII(Pt)∪6-31G**(L) geometries at the higher CCSD(T) level of theory using the same basis set [16]. For transition states geometry determination, quasi-Newton transit-guided (QSTN) computations were performed [17]. All DFT and CCSD(T)

calculations have been carried out using the GAUSSIAN03 program suite [18]. The natural bond orbital (NBO) population analysis was performed using Weinhold's methodology [19,20].

3. Results and discussion

The hydrosilylation, hydrocyanation, and hydroamination of ethene catalyzed by bis(hydrido-bridged)diplatinum complexes follow the general reaction route shown in Scheme 2 in analogy with the proposed mechanism for the hydrosilylation, hydrocyanation, and hydroamination of ethyne [2]. This mechanism consists of the following four steps: (i) coordination of the olefin to the monomeric T-shaped $[Pt(X)(PH_3)H]$ ($X = SiH_3$, CN, NH_2) species, (ii) insertion of the olefin into the platinum-hydride bond, (iii) reductive elimination of the final product and (iv) the oxidative addition process that regenerates the catalyst.

3.1. Catalytic cycle of the hydrosilylation of olefin catalyzed by the model "catalyst" 2

The molecular structures and selected structural parameters of all stationary points involved in the catalytic cycle of the hydrosilylation of ethene optimized at the B3LYP/LANL2DZ+BSII(Pt)∪6-31G**(L) level of theory are shown in Fig. 1, while the potential energy profile is given in Fig. 2.

At the entrance channel of the catalytic cycle an essential reaction takes place that generates the catalytically active species via an olefin addition to the precursor complex **1**. The latter is in equilibrium with the dimeric bis(hydrido-bridged)diplatinum complex, in solution which has been isolated and structurally characterized previously [21]. It was also experimentally found that the true active catalyst of hydrosilylation of alkenes and alkynes is the monomeric species [21]. The cleavage of the diplatinum complex yield the precursor **1** which adopt a planar T-shaped structure with the hydride in *trans* position to the phosphane spectator ligand. In the model catalyst **2** the olefin occupies a *trans* position to the SiH_3 ligand and adopts a coplanar orientation with respect to the coordination plane of the precursor complex **1**. The formation of intermediate **2** was computationally found to be exergonic by −15.4 (−25.0) kcal/mol at the B3LYP (CCSD(T)) levels of theory. The inclusion of entropic effects (ΔG) reduces the exergonicity to −3.7 kcal/mol.

Notably, the olefin addition elongates slightly the Pt–H bond by 0.5 pm. The Pt–Si bond is lengthened by 7.5 pm, as a result of the *trans*-influence of the ethene ligand, while

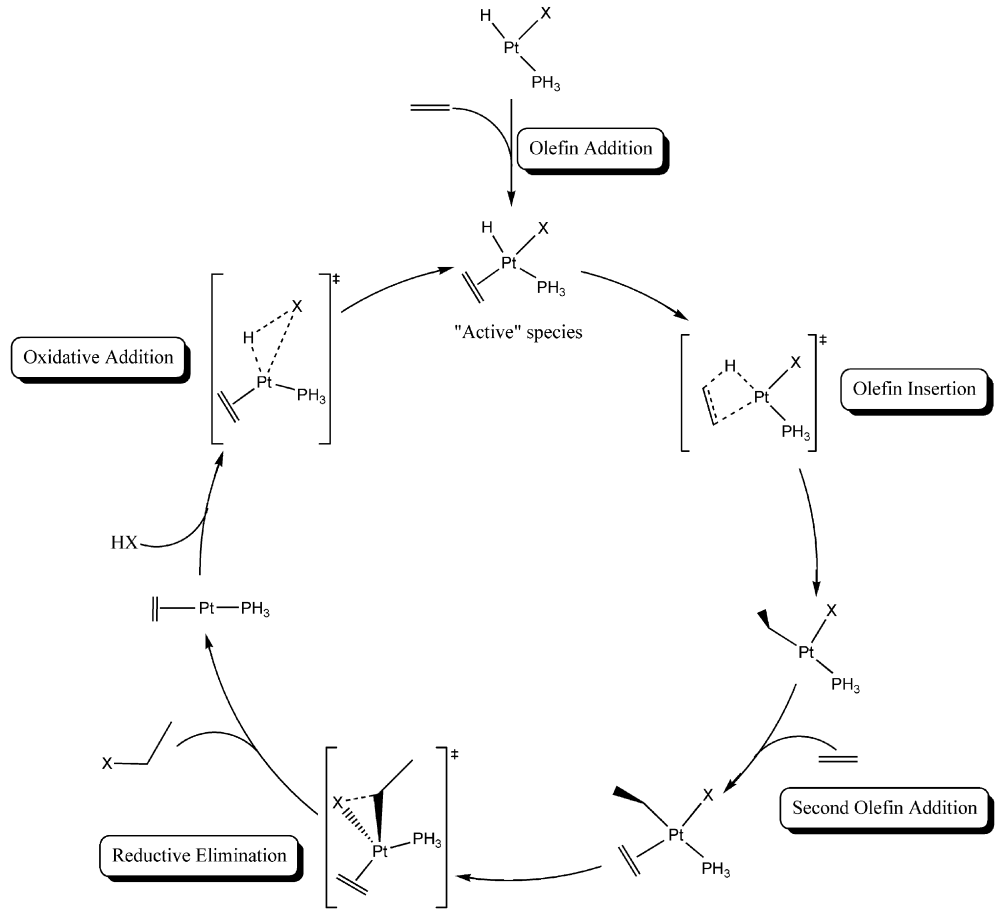

Scheme 2. General proposed catalytic cycle for the hydrosilylation, hydrocyanation, and hydroamination of ethene.

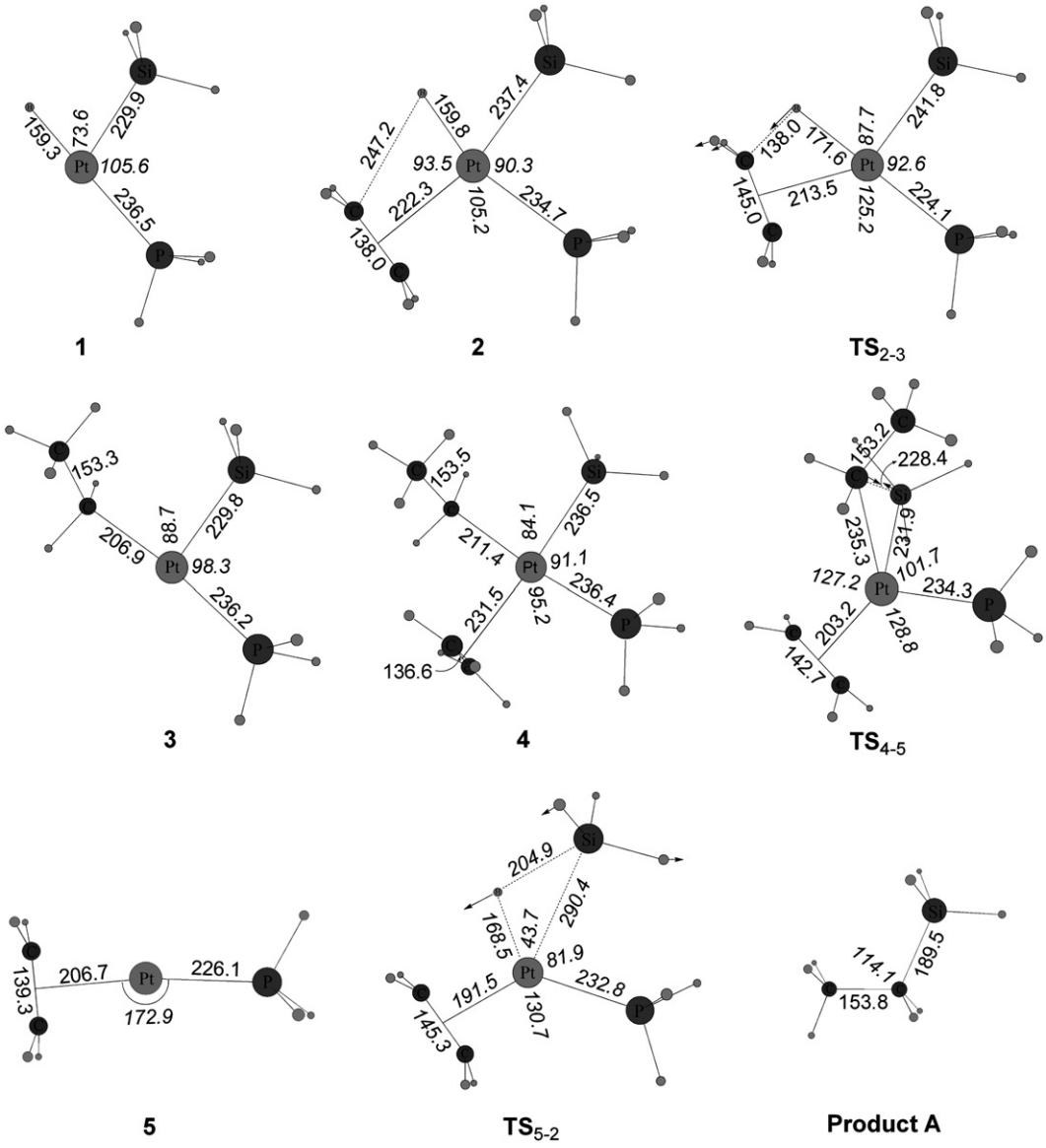

Fig. 1. Equilibrium structures of the relevant stationary points in the PES of the catalytic cycle for the hydrosilylation, with selected bond lengths (in pm) and angles (in deg).

the Pt–P one is shortened by 1.8 pm. These structural changes are reflected on the respective vibrational frequencies; the stretching vibrations of the Pt–H, Pt–Si and Pt–P bonds are predicted to be 2122, 342 and 289 cm^{-1}, respectively. Moreover, the coordination of the olefin to the platinum center results in the lengthening of the C═C double bond by 4.9 pm, with a ν(C═C) stretching vibrational frequency of 1590 cm^{-1}. The vibrational modes characterizing the coordination of the olefin with the Pt(II) metal center are the ν(Pt–C_2(*centroid*)) and ν_{as}(Pt–C_2) stretching vibrational modes that absorb at 236 and 382 cm^{-1}, respectively.

The σ(Pt–H) natural orbital is constructed from an $sd^{1.20}$ hybrid (54.45% d-character) on the platinum atom, $h_{Pt} = -0.672(6s)_{Pt} + 0.716(5d_{x^2-y^2})_{Pt} + 0.158(5d_z^2)_{Pt}$, interacting in-phase with the 1s orbital on the bridging hydride, thus having the form $\sigma(\text{Pt–H}) = 0.715h_{Pt} + 0.670s_H$. The Pt(II) metal center possess almost zero natural charge, while the terminal hydride ligand acquires a negative natural charge of −0.16 |e|.

In the next step of the catalytic cycle, the olefin inserts into the Pt–H bond, through $\mathbf{TS}_{2-3}$ to generate an unsaturated Pt-alkyl intermediate **3** with an activation barrier of 13.1 (15.2) kcal/mol in terms of ΔE_0 ($\Delta E_{CCSD(T)}^{\neq}$). The distance between the migrating hydride ligand and the nearest acceptor C atom of the coordinated ethene ligand has dramatically shortened by 96.9 pm with respect to the corresponding distance in complex **2**. The Pt–C(*centroid*) distance in $\mathbf{TS}_{2-3}$ is shortened by 8.8 pm, while the C–C bond length of the coordinated ethene molecule is further lengthened by 7.0 pm with respect to intermediate **2**. Analytical frequency calculations confirmed that $\mathbf{TS}_{2-3}$ is indeed a transition state characterized by a single

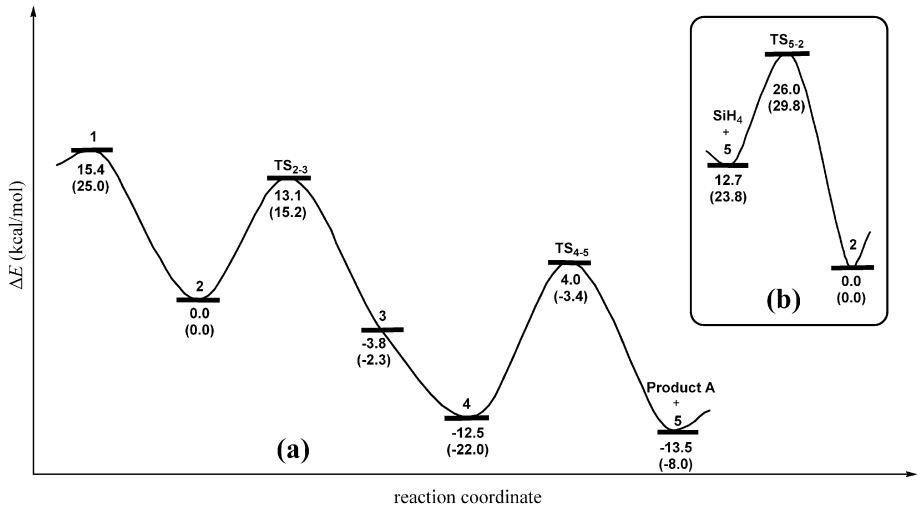

Fig. 2. (a) Reaction energy profile (ΔE_0 in kcal/mol) of the catalytic cycle of the hydrosilylation of ethene computed at the B3LYP/LANL2DZ+BSII(Pt)∪6-31G**(L) and CCSD(T)/LANL2DZ+BSII(Pt)∪6- 31G**(L)//B3LYP/LANL2DZ+BSII(Pt)∪6-31G**(L) (values in parenthesis) levels of theory; (b) the oxidative addition reaction energy profile that regenerates the catalytic species **2**.

imaginary frequency ($v_i = 406\ cm^{-1}$). In this case animation of the normal mode for the lone imaginary frequency displayed the desired nuclear displacement required for transferring hydride along with the nearest olefinic H atom of the coordinated H–C═C–H molecule. The olefin insertion reaction is predicted to be exergonic by −3.8 (−2.3) kcal/mol in terms of ΔE_0 at the B3LYP (CCSD(T)) levels for this pathway. The intermediate **3** is a coordinatively unsaturated 14e Pt(II) complex with a T-shaped structure (∠C–Pt–P = 172.9°), and a Si–Pt–C–C torsion angle of −68.0°. As expected, the saturated C–C bond in the Pt-alkyl intermediate is 15.3 pm longer than the unsaturated C═C of the π-adduct. In addition, the Pt–C_{alkyl} bond is predicted to be 27.9 pm shorter than the Pt–$C_{ethylene}$ bond. These structural changes are consistent with the transformation of an unsaturated alkene ligand to a saturated alkyl ligand. Following the formation of the unsaturated Pt-alkyl intermediate **3**, the subsequent step of the catalytic cycle involves coordination of a second olefin molecule to generate the coordinatively unsaturated 16e Pt(II) complex **4** (Fig. 1). The second olefin addition is predicted to be also exothermic by −8.5 (−19.7) kcal/mol at the B3LYP (CCSD(T)) levels of theory. The newly added olefin occupies the empty coordination site in *trans* position with respect to the SiH_3 ligand and prefers an almost vertical orientation with respect to the equatorial P–Pt–N–N plane. The addition of the olefin to the T-shaped Pt-alkyl intermediate induces an increase in the Pt–L bonds which are *cis* to the incoming olefin (about 2.1–3.6 pm) being the result of the competition with the other ligands in the equatorial plane to share the metal electron density. The next step in the catalytic cycle involves the reductive elimination process affording the product **A** ($H_3C–CH_2SiH_3$) and the catalytic species **5**. During the course of the reductive elimination process the silyl group is transferred to the acceptor C atom of the coordinated alkyl group via the transition state $\mathbf{TS}_{4–5}$ surmounting a relative low activation barrier of 16.5 (18.6) kcal/mol at the B3LYP (CCSD(T)) levels of theory. In $\mathbf{TS}_{4–5}$ the distance between the migrating silyl ligand and the nearest C atom of the acceptor alkyl group is 38.9 pm longer than the C–Si bond length in the final product **A**, whereas the C–C bond distance is slightly longer by 0.6 pm than the respective C–C bond length of product **A**. In the vibrational mode corresponding to the imaginary frequency of $\mathbf{TS}_{4–5}$, $v_i = 162\ cm^{-1}$, the dominant motions involve the transferring silyl group along with the nearest C atom of $H_3C–CH_2–$ ligand, as it is clearly shown in Fig. 1. Moreover, the reductive elimination step corresponds to an almost thermoneutral process (−1.0 kcal/mol) at the B3LYP level but is endergonic by 14.0 kcal/mol at the CCSD(T) level of theory. Finally, the oxidative addition of H–SiH_3 to intermediate **5** regenerating the "true" catalytic species **2** corresponds to an exothermic process, with exothermicity of −12.7 (−23.8) kcal/mol at the B3LYP (CCSD(T)) levels and surmounts a relative low activation barrier of 13.3 (6.6) kcal/mol in terms of ΔE_0 ($\Delta E_{CCSD(T)}^{\neq}$) (Fig. 2b). The transition state $\mathbf{TS}_{5–2}$ involves a loosely associated H–SiH_3 molecule interacting with the Pt(0) metal center in a κ^2-Si,H bonding mode, but with the Si–H bond strongly weakened, being 56.4 pm longer compared to the H–SiH_3 bond distance. In the vibrational mode corresponding to the imaginary frequency of $\mathbf{TS}_{5–2}$, $v_i = 479\ cm^{-1}$, the dominant motion involves the dissociation of the coordinated Si–H bond and the formation of the Pt–H and Pt–Si bonds. Upon, oxidative addition of H–SiH_3 to intermediate **5** the catalytic species **2** is regenerated and the catalytic cycle is completed.

In summary the rate-limiting step for the hydrosilylation of ethene is predicted to be the reductive elimination step in contrast with the hydrosilylation of ethyne where the hydride migration step was the rate-limiting step [2].

Moreover, the efficiency of the catalytic cycle of the hydrosilylation process is quantified by the energy span quantity, δE, of 39.5 (51.8) kcal/mol at the B3LYP (CCSD(T)) levels. Overall, the entire catalytic cycle of hydrosilylation of ethene is computed to be exothermic by −13.5 (−8.0) kcal/mol at B3LYP (CCSD(T)) levels of theory.

3.2. Catalytic cycle of the hydrocyanation of ethene catalyzed by the model "catalyst" 7

The molecular structures and selected structural parameters of all stationary points involved in the catalytic cycle of the hydrocyanation of ethene optimized at the B3LYP/LANL2DZ+BSII(Pt)∪6-31G**(L) level of theory are shown in Fig. 3, while the potential energy profile is given in Fig. 4.

The coordination of the olefin to the platinum center of the initially formed [Pt(H)(PH_3)(CN)] complex yielding the catalytically "active" [Pt(H)(PH_3)(CN)(η^2-C_2H_4)] species, corresponds to a exergonic process by −30.4 (−38.5) kcal/mol at the B3LYP (CCSD(T)) levels of theory. The inclusion of entropic effects (ΔG) reduces the exergonicity to −18.7 kcal/mol. Perusal of Fig. 3 illustrates the lengthening of the Pt–CN bond distance of intermediate **7** by 7.6 pm, as a result of the *trans*-influence of the ethene ligand, while the Pt–P bond length is shortened by 1.7 pm, with respect to the precursor **6**. These structural changes are reflected on the respective vibrational

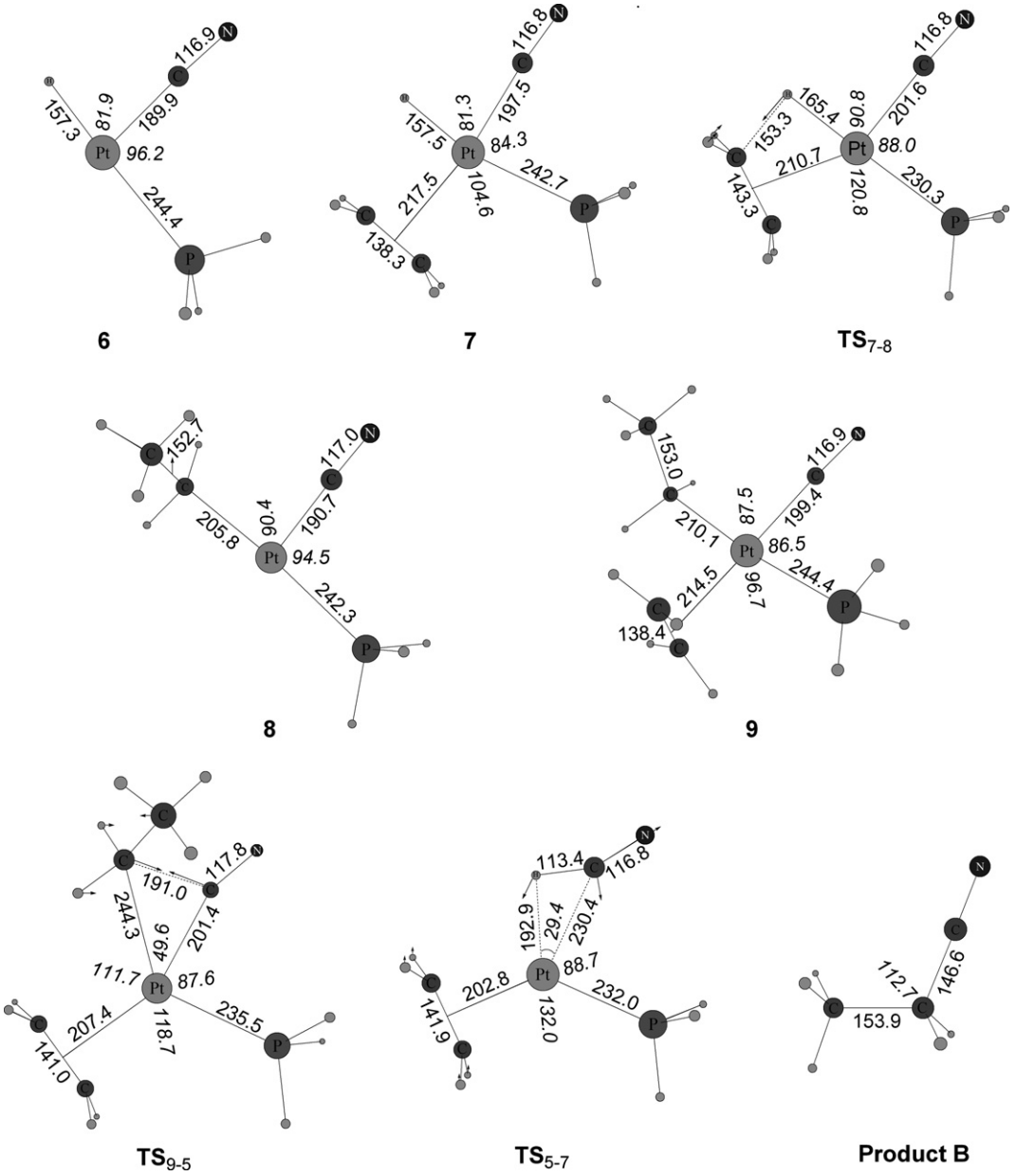

Fig. 3. Equilibrium structures of the relevant stationary points in the PES of the catalytic cycle for the hydrocyanation, with selected bond lengths (in pm) and angles (in deg).

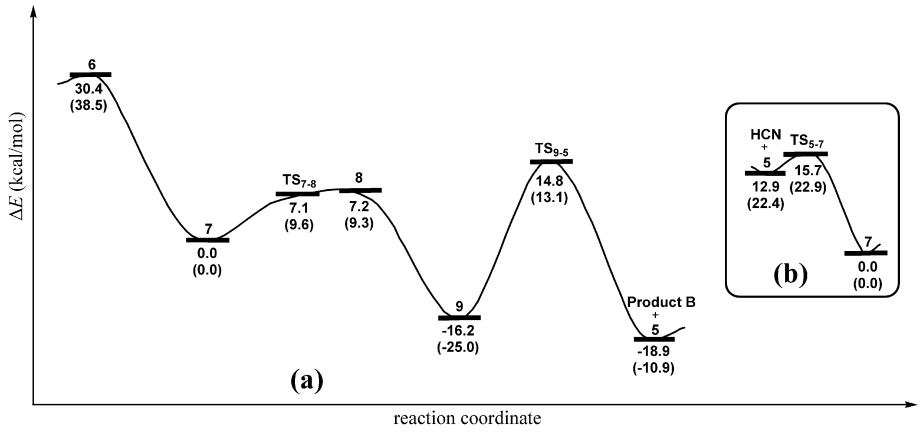

Fig. 4. (a) Reaction energy profile (ΔE_0 in kcal/mol) of the catalytic cycle of hydrocyanation computed at the B3LYP/LANL2DZ+BSII(Pt)∪6-31G**(L) and CCSD(T)/LANL2DZ+BSII(Pt)∪6-31G**(L)//B3LYP/LANL2DZ+BSII(Pt)∪6-31G**(L) (values in parenthesis) levels of theory; (b) the oxidative addition reaction energy profile that regenerates the catalytic species **7**.

frequencies; the stretching vibrations of the Pt–H, Pt–Si and Pt–P bonds are predicted to be 2202, 461 and 258 cm^{-1}, respectively.

In addition, the coordination of the olefin to the platinum metal center results in the lengthening of the C=C double bond by 5.2 pm, with a ν(C=C) stretching vibrational frequency of 1584 cm^{-1}. The vibrational modes characterizing the coordination of the olefin with the Pt(II) metal center is the ν(Pt–C_2(*centroid*)) stretching vibrational mode that absorbs at 306 cm^{-1}, respectively.

According to the NBO population analysis the σ(Pt–H) natural orbital is constructed from an $sd^{1.04}$ hybrid (50.93% d-character) on the platinum atom, $h_{Pt} = -0.699(6s)_{Pt} - 0.423(5d_{xy})_{Pt} + 0.561(5d_{x^2-y^2})_{Pt} - 0.118(5d_z^2)_{Pt}$, interacting in-phase with the 1s orbital on the bridging hydride, thus having the form $\sigma(Pt–H) = 0.729h_{Pt} + 0.684s_H$. The Pt(II) metal center acquires a positive natural charge of 0.25 |e|, while the terminal hydride ligand acquires a negative natural charge of only −0.04 |e|.

In the next step of the catalytic hydrocyanation cycle, the olefin inserts into the Pt–H bond, through $\mathbf{TS}_{7-8}$ yielding the unsaturated Pt-alkyl intermediate **8** with a low activation barrier demand of 7.1 (9.6) kcal/mol in terms of ΔE_0 ($\Delta E_{CCSD(T)}^{\neq}$). This activation barrier is slightly lower relative to that of the analogous step in the catalytic hydrosilylation cycle. The distance between the migrating hydride ligand and the nearest acceptor C atom of the coordinated ethene ligand has dramatically shortened by 80.1 pm with respect to the corresponding distance in complex **7**. The Pt–C(*centroid*) distance in $\mathbf{TS}_{7-8}$ is shortened by 6.8 pm, while the C–C bond distance of the coordinated ethene molecule is further lengthened by 5.0 pm with respect to intermediate **7**. Analytical frequency calculations confirmed that this species, $\mathbf{TS}_{7-8}$, is indeed a true transition state containing a single imaginary frequency ($v_i = 646$ cm^{-1}). Animation of the normal mode for the lone imaginary frequency displayed the desired nuclear displacement required for migrating hydride towards the nearest olefinic H atom of the coordinated ethene molecule. The olefin insertion reaction is predicted to be endergonic by 7.2 (9.3) kcal/mol in terms of ΔE_0 at the B3LYP (CCSD(T)) levels for this pathway. The intermediate **8** is a coordinatively unsaturated 14 e Pt(II) complex with a T-shaped structure (∠C–Pt–P = 175.2°) (Fig. 3). As expected, the saturated C–C bond in the Pt-alkyl intermediate is 14.4 pm longer than the unsaturated C=C bond of the π-adduct, **7**. In addition, the Pt–C_{alkyl} bond is predicted to be 29.0 pm shorter than the Pt–$C_{ethylene}$ bond. These structural changes are consistent with the transformation of the unsaturated alkene ligand to a saturated alkyl one. After formation of the unsaturated Pt-alkyl intermediate **8**, coordination of a second olefin molecule yields the coordinatively unsaturated 16 e Pt(II) complex **9**. The second olefin addition is predicted to be exothermic by −23.4 (−25.0) kcal/mol at the B3LYP (CCSD(T)) levels of theory. The newly added olefin occupies the empty position which is *trans* to the cyanide ligand preferring an almost vertical orientation with respect to the equatorial P–Pt–$C_{cyanide}$ plane. In the next step reductive elimination yields the product **B** ($H_3C–CH_2–CN$) and the catalytic species **5**, by overcoming a transition state, $\mathbf{TS}_{9-5}$, with a relative high activation barrier of 31.0 (38.1) kcal/mol at the B3LYP (CCSD(T)) levels of theory. Notably, $\mathbf{TS}_{9-5}$, is nonplanar (Fig. 3), the nonplanarity, probably is due to steric factors. In $\mathbf{TS}_{9-5}$ the cyanide ligand is inclined towards the alkyl group (C–Pt–$C_{cyanide}$ = 49.6°). The distance between the migrating cyanide ligand and the nearest C atom of the acceptor alkyl group is 44.4 pm longer than the C–CN bond length in the final product **B**, whereas the C–C bond distance is only 1.7 pm shorter than the respective C–C bond length of product **B**. In the vibrational mode corresponding to the imaginary frequency of $\mathbf{TS}_{9-5}$, $v_i = 414$ cm^{-1}, the dominant motions involve the migrating cyanide group along with the nearest C atom of $H_3C–CH_2–$ ligand (Fig. 4). The reductive elimination step in hydrocyanation cycle is predicted to be slightly exergonic by −2.7 kcal/mol at the B3LYP level and endergonic by 14.1 kcal/mol at the CCSD(T) level of theory.

Finally, the oxidative addition of H–CN to intermediate **5** regenerates the "true" catalytic species **7** via an exothermic process, with exothermicity of −12.9 (−22.4) kcal/mol at the B3LYP (CCSD(T)) levels and surmounting an almost barrierless activation energy of 12.6 (0.5) kcal/mol in terms of $\Delta E_0(\Delta E_{CCSD(T)}^{\neq})$. The transition state $\mathbf{TS}_{5-7}$ involves a loosely associated H–CN molecule interacting with the Pt(0) metal center in a κ^2-$C_{cyanide}$, H bonding mode, but with the C–H bond slightly weakened, being 9.9 pm longer compared to the H–CN bond distance. The imaginary frequency of $\mathbf{TS}_{5-7}$, $v_i = 141\ cm^{-1}$, reflects the dominant motion that involves the dissociation of the coordinated H–CN bond and the formation of the Pt–H and Pt–$C_{cyanide}$ bonds.

In summary the rate-limiting step for the catalytic hydrocyanation of ethene cycle is predicted to be the analogous to that of the respective catalytic hydrosilylation cycle. Moreover the efficiency of the catalytic cycle of the hydrocyanation process is quantified by the energy span quantity, δE, of 34.6 (47.9) kcal/mol at the B3LYP (CCSD(T)) levels. Overall the entire catalytic cycle of hydrocyanation of ethene is predicted to be more exothermic than the catalytic hydrosilylation cycle, with the total exothermicity being −18.9 (−10.9) kcal/mol at B3LYP (CCSD(T)) levels of theory.

3.3. Catalytic cycle of the hydroamination of ethene catalyzed by the model "catalyst" 11

The molecular structures and selected structural parameters of all stationary points involved in the catalytic cycle of the hydroamination of ethene optimized at the B3LYP/LANL2DZ+BSII(Pt)∪6-31G**(L) level of theory are shown in Fig. 5, while the potential energy profile is given in Fig. 6.

Molecule **11** (Fig. 5) serves as the catalytically "active" complex for the hydroamination of olefins. It is formed by the addition of an ethene molecule to the precursor complex **10**. In species **11** the coordinated olefin occupies a *trans* position to the amido (NH_2) ligand preferring a coplanar orientation with respect to the coordination plane of the precursor Pt(II) complex. The formation of intermediate **11** is predicted to be exergonic by −28.7 (−36.9) kcal/mol at the B3LYP (CCSD(T)) levels of theory. The inclusion of entropic effects (ΔG) reduces the exergonicity to −16.9 kcal/mol. Noteworthy the exergonicity of the first step of the hydroamination process is comparable to that of the hydrocyanation one.

Perusal of Fig. 5 indicates that the olefin addition does not affect the Pt–H bond length. However, the Pt–N bond is lengthened by 5.5 pm, as a result of the *trans*-influence of the ethene ligand, while the Pt–P one is shortened by 1.4 pm. These structural changes are reflected on the respective vibrational frequencies; the stretching vibrations of the Pt–H, Pt–N and Pt–P bonds are predicted to be 2186, 549 and 230 cm^{-1}, respectively.

Notably upon coordination of the olefin molecule to the platinum center the C=C double bond is lengthening by 6.3 pm, while the ν(C=C) stretching vibrational frequency occurs at 1282 cm^{-1}. Moreover, in the intermediate **11** the P–Pt–H nuclear framework deviates from linearity by 20.1°. The vibrational modes characterizing the coordination of the olefin with the Pt(II) metal center are the ν(Pt–C_2(*centroid*)) and ν_{as}(Pt–C_2) stretching vibrational modes that absorb at 334 and 455 cm^{-1}, respectively.

According to NBO analysis, the σ(Pt–H) natural orbital is constructed from an $sd^{0.79}$ hybrid (45.05% d-character) on the platinum atom, $h_{Pt} = -0.746(6s)_{Pt} + 0.647(5d_{xy})_{Pt} + 0.121(5d_z^2)_{Pt}$, interacting in-phase with the 1s orbital on the bridging hydride, thus having the form σ(Pt–H) = $0.699h_{Pt} + 0.716s_H$. Notice the decrease of the d character in the sd hybrid of Pt(II) with a concomitant increase of the s_H contribution to the σ(Pt–H) bonding interaction in **11** than in **7** and **2** complexes. The Pt(II) metal center acquires a positive natural charge of 0.37 |e|, while the terminal hydride ligand acquires a negative natural charge of −0.10 |e|.

The next step of the catalytic cycle is the olefin insertion into the Pt–H bond, through $\mathbf{TS}_{11-12}$ to generate the unsaturated Pt-alkyl intermediate **12** with a moderate activation barrier of 11.7(14.5) kcal/mol in terms of ΔE_0 ($\Delta E_{CCSD(T)}^{\neq}$). The activation barrier is comparable to that of the hydrosilylation process, but higher than the corresponding activation barrier of the catalytic hydrocyanation cycle. The structural features of the transition state $\mathbf{TS}_{11-12}$ are similar to those of $\mathbf{TS}_{2-3}$ and $\mathbf{TS}_{7-8}$. The distance between the migrating hydride ligand and the nearest acceptor C atom of the ethene ligand has extremely shortened by 86.5 pm with respect to the corresponding distance in complex **11**. The Pt–C(*centroid*) distance in $\mathbf{TS}_{11-12}$ is shortened by 3.0 pm, while the C–C bond distance of the coordinated ethene molecule is further lengthened by 5.1 pm with respect to intermediate **11**. Analytical frequency calculations confirmed that $\mathbf{TS}_{11-12}$ is indeed a true transition state containing a single imaginary frequency ($v_i = 667\ cm^{-1}$). The animation of the normal mode for the lone imaginary frequency displayed the desired nuclear displacement required for transferring hydride along with the nearest olefinic H atom of the coordinated $H_2C{=}CH_2$ molecule. The olefin insertion process is predicted to be endothermic by 7.8 (5.3) kcal/mol in terms of ΔE_0 ($\Delta E_{CCSD(T)}^{\neq}$) at the B3LYP (CCSD(T)) levels for this pathway. The intermediate **12** is a coordinatively unsaturated 14e Pt(II) complex with a T-shaped structure (∠C–Pt–P = 179.0°), and a N–Pt–C–C torsion angle of −42.6°. As expected, the saturated C–C bond in the Pt-alkyl intermediate is more than 10 pm longer than the unsaturated C=C of the π-adduct. In addition, the Pt–C_{alkyl} bond is predicted to be 17.5 pm shorter than the Pt–$C_{ethylene}$ bond. Next to the formation of the unsaturated Pt-alkyl intermediate **12**, follows the subsequent step of the catalytic cycle that involves the coordination of a second olefin molecule to yield the coordinatively unsaturated 16e Pt(II) complex **13.** The second olefin addition is predicted to be highly exothermic by −28.6 (−41.2) kcal/mol at the B3LYP

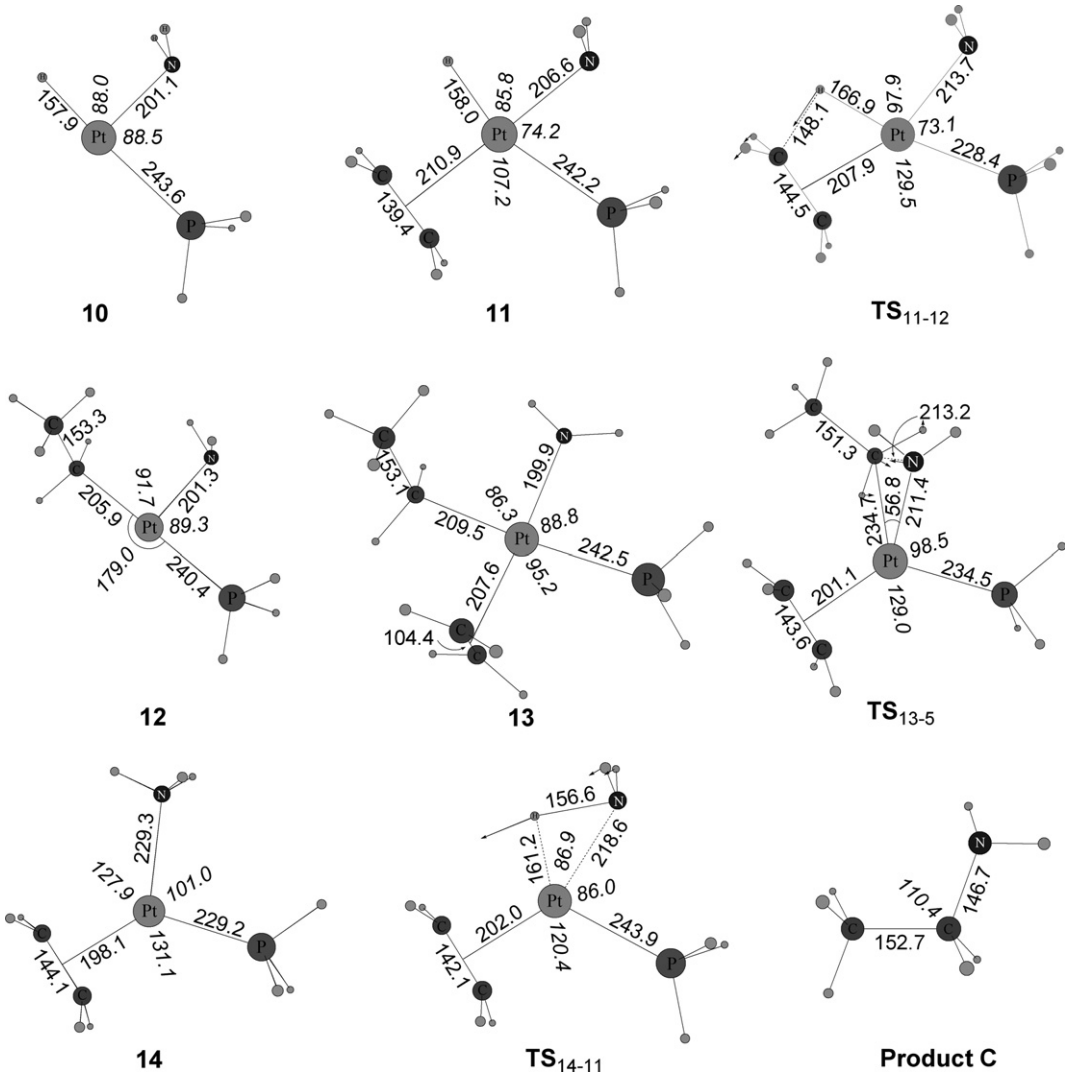

Fig. 5. Equilibrium structures of the relevant stationary points in the PES of the catalytic cycle for the hydroamination, with selected bond lengths (in pm) and angles (in deg).

(CCSD(T)) levels of theory, respectively. The newly incoming olefin molecule occupies the empty coordination site in *trans* position to the NH_2 ligand adopting an almost vertical orientation with respect to the equatorial plane of the P–Pt–N. The addition of the olefin to the T-shaped Pt-alkyl intermediate induces an increase in the Pt–L bonds which are *cis* to the incoming olefin (about 2.1–3.6 pm) which probably as a result of the competition with the other ligands in the equatorial plane for the metal electron density.

In the next step of the catalytic hydroamination cycle the product **C** (H_3C–CH_2NH_2) and the catalytic species **5** are formed via a reductive elimination process. During the course of the reductive elimination process the amido ligand is transferred to the acceptor C atom of the coordinated alkyl group via the transition state $\mathbf{TS}_{13-5}$. The energy demand (Fig. 6) illustrates that the reductive elimination process (activation barrier of 39.7 (46.9) kcal/mol) is less favorable kinetically than the hydrocyanation reductive elimination step (barrier of 30.0 (38.1) kcal/mol) and much less favorable than the hydrosilylation reductive elimination step (barrier of 16.5 (18.6) kcal/mol). In $\mathbf{TS}_{13-5}$ the amido ligand is inclined towards the alkyl group by 29.5° (N–Pt–C = 56.8°). The distance between the migrating amido ligand and the nearest C atom of the acceptor alkyl group is 66.5 pm longer than the C–N bond length in the final product **C**, whereas the C–C bond distance is only 1.4 pm longer than the respective C–C bond length of product **C**. In the vibrational mode corresponding to the imaginary frequency of $\mathbf{TS}_{13-5}$, $\nu_i = 438\ \mathrm{cm}^{-1}$, the dominant motions involve the transferring amido group along with the nearest C atom of H_3C–CH_2- ligand. The reductive elimination in hydroamination is predicted to be exergonic at the B3LYP level ($\Delta E_0 = -7.3$ kcal/mol) but it is endergonic ($\Delta E_0 = 8.7$ kcal/mol) at the CCSD(T) level.

The subsequent step of the catalytic cycle is the addition of the NH_3 to intermediate **5**. This is an additional step,

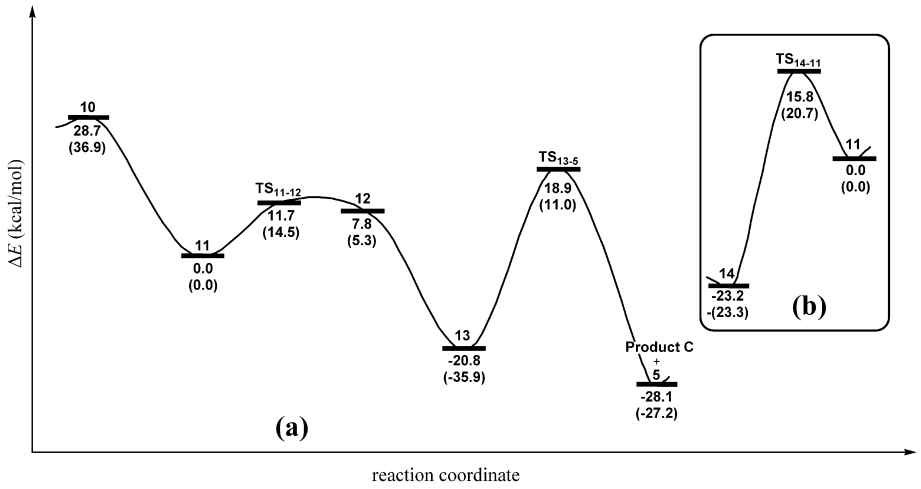

Fig. 6. (a) Reaction energy profile (ΔE_0 in kcal/mol) of the catalytic cycle of hydroamination computed at the B3LYP/LANL2DZ+BSII(Pt)∪6-31G**(L) and CCSD(T)/LANL2DZ+BSII(Pt)∪6-31G**(L)//B3LYP/LANL2DZ+BSII(Pt)∪6-31G**(L) (values in parenthesis) levels of theory; (b) the oxidative addition reaction energy profile that regenerates the catalytic species **11**.

which has not been included in the catalytic hydrosilylation and hydrocyanation cycles, for the lone pair on the nitrogen of NH_3 ligand could support coordination with the unsaturated intermediate **5** to yield complex **14**. This is not the case for the SiH_4 and HCN substrates, for these ligands have no lone pair to bind with the metal center. The intermediate **14** adopt an almost trigonal structure with NH_3 being loosely coordinated with the metal center (Fig. 5).

In the final step oxidative addition of H–NH_2 regenerates the ''true'' catalytic species **11**. This reaction, in contrast to the catalytic hydrosilylation and hydrocyanation cycles, corresponds to an endothermic process, with endothermicity of 23.2 (23.3) kcal/mol at the B3LYP (CCSD(T)) levels and surmounts a remarkably high activation barrier of 39.0 (44.0) kcal/mol in terms of ΔE_0 ($\Delta E_{CCSD(T)}^{\neq}$). These activation barriers are much higher than the corresponding oxidative addition barriers of the hydrosilylation and hydrocyanation processes. The transition state $\mathbf{TS}_{14-11}$ involves a loosely associated H–NH_2 molecule interacting with the Pt(0) metal center in a κ^2-N,H bonding mode, but with the N–H bond strongly weakened. The imaginary frequency of $\mathbf{TS}_{14-11}$, $v_i = 925\ cm^{-1}$, refers to the dominant motion involving dissociation of the coordinated N–H bond and formation of the Pt–H and Pt–N bonds. Upon, oxidative addition of H–NH_2 to intermediate **14** the catalytic species **11** is regenerated and the catalytic cycle is completed.

In summary the geometric and energetic profile of the hydroamination of ethene closely resembles those of the respective hydrosilylation and hydrocyanation reactions. However, the hydroamination process is less favored both thermodynamically and kinetically, since the two critical rate-limiting steps, namely the reductive elimination and the oxidative addition steps are less favored. Therefore these platinum complexes are predicted to be less efficient catalysts for hydroamination of unsaturated substrates. This is further substantiated by the computed δE values of 57.7 (67.4) at the B3LYP (CCSD(T)) levels, which are higher than those of the hydrosilylation and hydrocyanation processes. This could be due to the stabilization of the lowest energy species in the cycle of the hydroamination process. Overall, the entire catalytic cycle of hydroamination of olefin is predicted to be more exothermic than the catalytic hydrosilylation and hydrocyanation cycles, with the total exothermicity being −38.8 (−46.7) kcal/mol at B3LYP (CCSD(T)) levels of theory.

4. Conclusions

We have performed a molecular-level computational investigation of the mechanism of hydrosilylation, hydrocyanation and hydroamination of ethene catalyzed by bis(hydrido-bridged)diplatinum complexes. Our calculations show that the catalytically ''active'' species are the 16e coordinatively unsaturated mononuclear [Pt(X)(H)-(PH_3)(η^2-C_2H_4)] (X = SiH_3, CN, NH_2) species formed upon addition of the ethene molecule on the monomeric [Pt(X)(H)(PH_3)] precursors. Overall, the reactions can be partitioned into three main sections: (i) the hydride migration to the acceptor C atom of the coordinated ethene substrate, (ii) the reductive elimination of the hydrosilylated, hydrocyanated or hydroaminated product and (iii) the oxidative addition process that regenerates the catalytic species. Analysis of the computed potential energy surfaces allowed us to identify effective barriers, consisting of combined elementary steps, for these three stages of the hydrosilylation, hydrocyanation and hydroamination reactions. The computed activation barriers ΔE_0 ($\Delta E_{CCSD(T)}^{\neq}$) for the rate-determining steps were found to be 13.1, 16.5 and 13.3 kcal/mol for the hydrosilylation, 7.1, 31.0 and 2.8 kcal/mol for the hydrocyanation and 11.7, 39.7 and 39.0 kcal/mol for the hydroamination reactions. The rate-limiting steps differ in the three catalytic processes, being

step (ii) in hydrosilylation and hydrocyanation, and both steps (ii) and (iii) in hydroamination. The efficiency of the catalytic cycles determined by the energy span quantity, δE, follows the trend: hydrocyanation $\approx$ hydrosilylation $>$ hydroamination. Moreover, the hydrosilylation, hydrocyanation and hydroamination of ethene catalyzed by bis(hydrido-bridged)diplatinum complexes are predicted to be exothermic by -13.5 (-8.0), -18.9 (-10.9) and -38.8 (-46.7) kcal/mol, respectively, at the B3LYP (CCSD(T)) levels of theory, in line with existing experimental observations in the case of hydrosilylation. Sound theoretical treatment should represent a potent tool for further development of platinum-based catalysts in particular for the hydrocyanation and hydroamination of unsaturated substrates, processes that are of potential synthetic interest.

Appendix A. Supplementary material

Supplementary data associated with this article can be found, in the online version, at doi:10.1016/j.jorganchem.2007.08.007.

References

[1] A.R. Chianese, S.J. Lee, M.R. Gagn, Angew. Chem., Int. Ed. 46 (2007) 4042.
[2] C.A. Tsipis, C.E. Kefalidis, Organometallics 25 (2006) 1696.
[3] (a) S. Kozuch, S. Shaik, J. Am. Chem. Soc. 128 (2006) 3355;
(b) S. Kozuch, C. Amatore, A. Jutand, S. Shaik, Organometallics 24 (2005) 2319;
(c) C. Amatore, A. Jutand, J. Organomet. Chem. 576 (1999) 254.
[4] R. Schmid, W.A. Herrmann, G. Frenking, Organometallics 16 (1997) 701.
[5] (a) K. Tatsumi, R. Hoffmann, A. Yamamoto, J.K. Stille, Bull. Chem. Soc. Jpn. 54 (1981) 1857;
(b) J.L. Low, W.A. Goddard, J. Am. Chem. Soc. 108 (1986) 6115;
(c) J.L. Low, W.A. Goddard, Organometallics 5 (1986) 609;
(d) N. Koga, K. Morokuma, Organometallics 10 (1991) 946;
(e) M.R.A. Blomberg, P.E.M. Siegbahn, U. Nagashina, J. Wennerberg, J. Am. Chem. Soc. 113 (1991) 424;
(f) P.E.M. Siegbahn, M.R.A. Blomberg, J. Am. Chem. Soc. 114 (1992) 10548;
(g) S. Sakaki, M. Ieki, J. Am. Chem. Soc. 115 (1993) 2373;
(h) S. Sakaki, M. Ogawa, Y. Musashi, T. Arai, Inorg. Chem. 33 (1994) 1660;
(i) S. Sakaki, N. Mizoe, Y. Musashi, B. Biswas, M. Sugimoto, J. Phys. Chem. A 102 (1998) 8027;
(j) G.S. Hill, R.J. Puddephatt, Organometallics 17 (1998) 1478;
(k) Z. Cao, M.B. Hall, Organometallics 19 (2000) 3338;
(l) A. Sundermann, O. Uzan, D. Milstein, J.M.L. Martin, J. Am. Chem. Soc. 122 (2000) 7095;
(m) A. Sundermann, O. Uzan, J.M.L. Martin, Organometallics 20 (2001) 1783.
[6] (a) A. Dedieu, Chem. Rev. 100 (2000) 543;
(b) D.G. Musaev, K. Morokuma, Top. Catal. 7 (1999) 107;
(c) P.E.M. Siegbahn, in: P.W.N.M. van Leeuwen, J.H. van Lenthe, K. Morokuma (Eds.), Theoretical Aspects of Homogeneous Catalysis, Applications of Ab Initio Molecular Orbital Theory, Kluwer Academic, Dordrecht, The Netherlands, 1995;
(d) N. Koga, K. Morokuma, Chem. Rev. 91 (1991) 823.
[7] V.P. Ananikov, D.G. Musaev, K. Morokuma, J. Am. Chem. Soc. 124 (2002) 2839.
[8] (a) A.D. Becke, J. Chem. Phys. 96 (1992) 2155;
(b) A.D. Becke, J. Chem. Phys. 98 (1993) 5648.
[9] C. Lee, W. Yang, R.G. Parr, Phys. Rev. B37 (1988) 785.
[10] S.H. Vosko, L. Wilk, M. Nusair, Can. J. Phys. 58 (1980) 1200.
[11] J. Baker, M. Muir, J. Andzelm, A. Scheiner, in: B.B. Laird, R.B. Ross, T. Ziegler (Eds.), Chemical Applications of Density-Functional Theory, ACS Symposium Series, vol. 629, American Chemical Society, Washington, DC, 1996.
[12] L.A. Curtiss, K. Raghavachari, P.C. Redfern, J.A. Pople, J. Chem. Phys. 106 (1997) 1063.
[13] G. Frenking, I. Antes, M. Böhme, S. Dapprich, A.W. Ehlers, V. Jonas, A. Neuhaus, M. Otto, R. Stegmann, A. Veldkamp, S.F. Vyboishchikov, in: K.B. Lipkowitz, D.B. Boyds (Eds.), Reviews in Computational Chemistry, VCH, New York, 1996, p. 63.
[14] (a) P.J. Hay, W.R.J. Wadt, Chem. Phys. 82 (1985) 270;
(b) W.R. Wadt, P. J Hay, J. Chem. Phys. 82 (1985) 284;
(c) P.J. Hay, W.R. Wadt, J. Chem. Phys. 82 (1985) 299.
[15] (a) B.J. Lynch, P.L. Fast, M. Harris, D.G. Truhlar, J. Phys. Chem. A 104 (2000) 4811;
(b) B.J. Lynch, D.G. Truhlar, J. Phys. Chem. A 105 (2001) 2936;
(c) J. Poater, M. Sola, M. Duran, L. Robles, Phys. Chem. Chem. Phys. 4 (2002) 722.
[16] J.A. Pople, M.P. Head-Gordon, K. Raghavachari, J. Chem. Phys. 87 (1987) 5968.
[17] M.P. Head-Gordon, M.J. Frisch, Chem. Phys. Lett. 153 (1988) 503.
[18] M.J.T. Frisch et al., Gaussian 03, Revision B. 02, Gaussian, Inc.: Pittsburgh PA, 2003. See Supporting Information for remaining 80 authors.
[19] A.E. Reed, L.A. Curtiss, F. Weinhold, Chem. Rev. 88 (1988) 899.
[20] F. Weinhold, in: P.v.R. Schleyer (Ed.), The Encyclopedia of computational Chemistry, John Wiley & Sons, Chichester, 1988, p. 1792.
[21] (a) M. Green, J.A.K. Howard, J. Proud, J.L. Spencer, F.G.A. Stone, C.A. Tsipis, J. Chem. Soc., Chem. Commun. (1976) 671;
(b) M. Ciriano, M. Green, J.A.K. Howard, J. Proud, J.L. Spencer, F.G.A. Stone, C.A. Tsipis, J. Chem. Soc., Dalton Trans. (1976) 801;
(c) M. Ciriano, M. Green, J.A.K. Howard, M. Murray, J.L. Spencer, F.G.A. Stone, C.A. Tsipis, Advances in Chemistry Series No 167, ACS 1976, p 112;
(d) M. Green, J.L. Spencer, F.G.A. Stone, C.A. Tsipis, J. Chem. Soc., Dalton Trans. (1977) 1519;
(e) M. Green, J.L. Spencer, F.G.A. Stone, C.A. Tsipis, J. Chem. Soc., Dalton Trans. (1977) 1525;
(f) C.A. Tsipis, J. Organomet. Chem. 187 (1980) 427;
(g) C.A. Tsipis, J. Organomet. Chem. 188 (1980) 53.